A Novel Ratiometric Electrochemical Biosensor Based on a Split Aptamer for the Detection of Dopamine with Logic Gate Operations

Ting Guo, Changtong Wu, Andreas Offenhäusser, and Dirk Mayer*

A novel dual-signal ratiometric electrochemical biosensor based on a split aptamer is developed. A common shortcoming of amperometric aptamer sensors is unspecific signaling due to ssDNA conformational flexibility. Herein, a ratiometric detection using two competitive redox-labeled aptamer strands is proposed. The neurotransmitter dopamine (DA) is chosen as a model target due to its importance for signal processing in the central nervous system. A DA aptamer is split into two parts, S1 and S2, where strand S1 is tethered to the electrode, whereas the second strand is labeled with methylene blue (MB) and acts as a redox reporter. Another ssDNA strand (CS1) tagged with anthraquinone (AQ) is introduced, which is complementary to strand S1 and reports on surface-tethered strands that remain in its virgin state. In the presence of DA, CS1 is released from the surface due to the formation of S1–S2–DA complexes, resulting in decreasing AQ and increasing MB Faraday currents. Furthermore, logic gate operations can be performed to either improve signal reliability or enlarge the detection range. This proof-of-concept study demonstrates that the splitting of a full aptamer into two parts together with the use of complementary ratiomeric tests can improve the reliability of the sensor response.

1. Introduction

Electrochemical aptamer-based biosensors (E-AB) have attracted great interest due to their simplicity, robustness, reusability, and low cost, while being also highly sensitive and selective. These sensors have proven to be able to detect a variety of different analytes such as small molecules, proteins, inorganic ions, or even cells.[1–9] E-ABs traditionally utilize target-induced conformational changes as transducer principles to generate a sensor signal. This conformational change may alter the distance of the redox tag to the electrode surface, producing current signal change.[10–14] Yu and Lai reported a "signal-on" electrochemical biosensor based on target-induced changes in the conformation and flexibility of a methylene blue (MB)-modified aptamer for detection of ampicillin.[15,16] However, this target-induced change in conformation facilitates in some cases only small sensor signals, and nonanalyte-related effects can alter the sensor response. Furthermore, the deterioration of the sensing surface due to hard-to-avoid variations in electrode areas, DNA loading densities, and nontarget-induced reagent degradation or dissociation may generate interfering signal changes.[17–19] This potentially affects the reproducibility and reliability of analyte detection.

Ratiometric detection approaches have been widely used in the fluorescence analysis of biomolecules.[20,21] Deng et al. developed a fluorescence resonance energy transfer (FRET)-based ratiometric biosensor for the detection of kanamycin.[22] Interestingly, ratiometric detection schemes have also recently been introduced for electrochemical biosensors.[23–27] Ratiometric biosensors with dual-signal outputs have the capability to efficiently overcome potential interferences caused by complex experimental conditions and improve reproducibility and detection accuracy. Li et al. developed a dual-reporter method to correct the baseline drift caused by a complex analyte composition.[28] A sensing reporter and reference reporter were modified at the distal and proximal end of the aptamer, respectively. The sensing reporter only responded to target-induced conformational changes. The reference reporter was independent of conformational changes and indicated the number of receptor molecules on the sensor. This method largely eliminated the drift caused by the complex sample matrix. Li et al. constructed a ratiometric electrochemical sensor based on a mismatched catalytic hairpin assembly for the detection of microRNA.[29] In addition, recent work demonstrated that the signal background could be reduced by splitting the aptamer.[30–32] Zheng et al. developed a DNA nanoprobe for ATP based on FRET between the strands of a split

Dr. T. Guo
College of Food Science
Southwest University
Chonqing 400715, P. R. China

Dr. T. Guo, C. Wu, Prof. A. Offenhäusser, Dr. D. Mayer
Institute of Biological Information Processing
Bioelectronics (IBI-3)
Forschungszentrum Jülich GmbH
Jülich 52425, Germany
E-mail: dirk.mayer@fz-juelich.de

The ORCID identification number(s) for the author(s) of this article can be found under https://doi.org/10.1002/pssa.201900924.

aptamer.[33] Our group reported on a new sensor based on a split aptamer for ATP detection with improved limit of detection (LOD).[34,35] In this work, we detail on the development of a ratiometric electrochemical biosensor based on a split aptamer for the detection of dopamine (DA). DA is an important neurotransmitter and plays a crucial role in many brain functions and behavioral responses. The disorder of DA levels could be related to neuronal diseases, such as Parkinson's disease, schizophrenia, and attention-deficit hyperactivity disorder. Elevated levels of DA are usually observed for patients with drug addiction. Furthermore, DA is involved in controlling the cardiovascular, renal, and hormonal systems of humans. In these strongly diverse systems, the level of DA varies from sub-nM levels in cerebrospinal fluid for patients with Parkinson's disease[36] to high micrometer levels in the caudate nucleus.[37] The extraordinary importance of DA as a biomarker and the different requirements of the various samples have stimulated numerous works to engineer biosensors based on a variety of transducer principles sensitive in different concentration ranges. For reference, please see the review of Jackowska and Krysinski.[38] Among all these different sensor concepts, we want to highlight the work of Kim et al. who engineered an in vitro sensor for measuring the release of neurotransmitters from dopaminergic cells, which potentially can be used for toxicity assessments or testing the efficacy of newly developed anticancer drugs.[39] Here, a previously reported ssDNA full aptamer receptor that is capable of binding DA was split into two parts, S1 and S2. The working principle of our ratiometric electrochemical biosensor is shown in **Figure 1**. Strand S1 containing a thiol is tethered to the electrode and is free of redox tags. In contrast, the second strand is labeled with MB and acts as a redox reporter for the binding of the analyte. In addition, a ssDNA strand (CS1) tagged with anthraquinone (AQ) is introduced, which is complementary to strand S1. CS1 is not involved in target binding but competes with S2 + DA on the association with S1. Consequently, the CS1-associated redox signal of AQ reports on the surface-tethered receptor strands that remain in its virgin state. The hybridization between CS1 and S1 assures that the AQ redox probe is in close proximity to the electrode and enables an evident redox signal. In the presence of DA, CS1 releases from the electrode surface due to the formation of the S1–S2–DA complex, resulting in the decrease in AQ and increase in MB currents.

2. Results and Discussion

2.1. Electrochemical Characterization of the Biosensor

We used cyclic voltammetry (CV) and electrochemical impedance spectroscopy (EIS) to monitor the biosensor fabrication and assembly processes on a gold chip with 5×10^{-3} M $[Fe(CN)_6]^{3-/4-}$ as a redox probe. Compared with the bare gold chip (curve a), the peak current decreased significantly and the peak width increased after immobilizing S1 on the gold chip (curve b), as shown in **Figure 2**A, indicating a blocking of charge transfer due to the binding of the negatively charged aptamer strands. After the addition of mercapto-1-hexanol (MCH), the aptamer uncovered sites were also blocked, resulting in a further decrease of the peak current and increase in peak-to-peak separation (curve c). In the presence of DA and the second part of the split aptamer S2, the peak current decreased even further (curve d) due to the formation of S1–DA–S2 sandwich structures.

The immobilization process was also evaluated by impedance spectroscopy recorded at the standard electrode potential of the redox probe at 220 mV (saturated calomel electrode) and presented as a Nyquist plot. The semicircle diameter corresponds to the electron-transfer process. The increase in diameter reflects
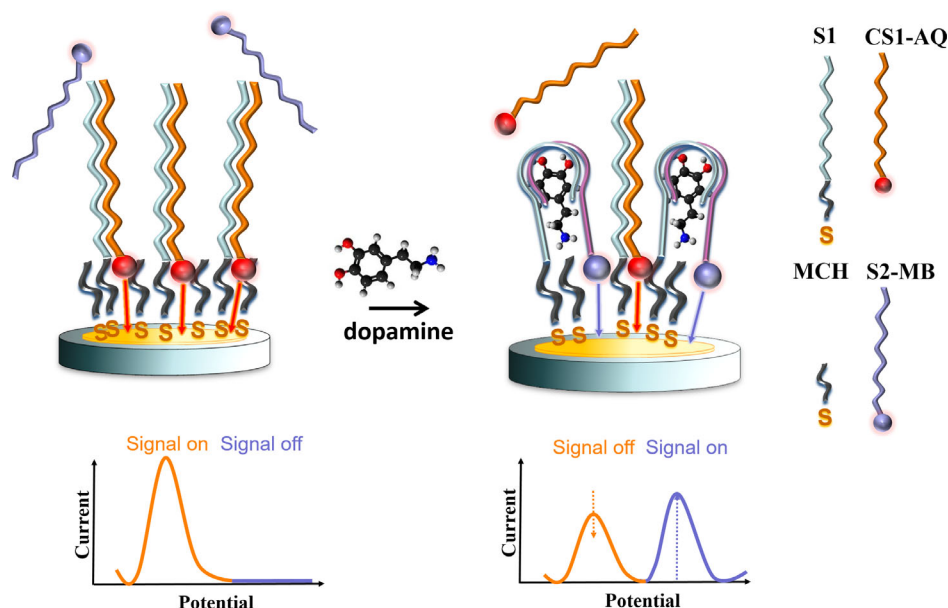

Figure 1. A scheme of the ratiometric electrochemical biosensor for the detection of DA. Top illustrates the competitive binding of the redox tagged ssDNA molecules CS1-AQ and S2-MB to the surface-tethered capture strand S1. Bottom line shows schematic SWV curves corresponding to the different sensor configurations above. Left, DA-free situation: only the CS1-AQ redox signal is present; right, after addition of DA: both AQ and MB signals can be registered because S2-MB partially substituted CS1-AQ. MCH was used as backfill molecules to prevent unspecific sensor responses.
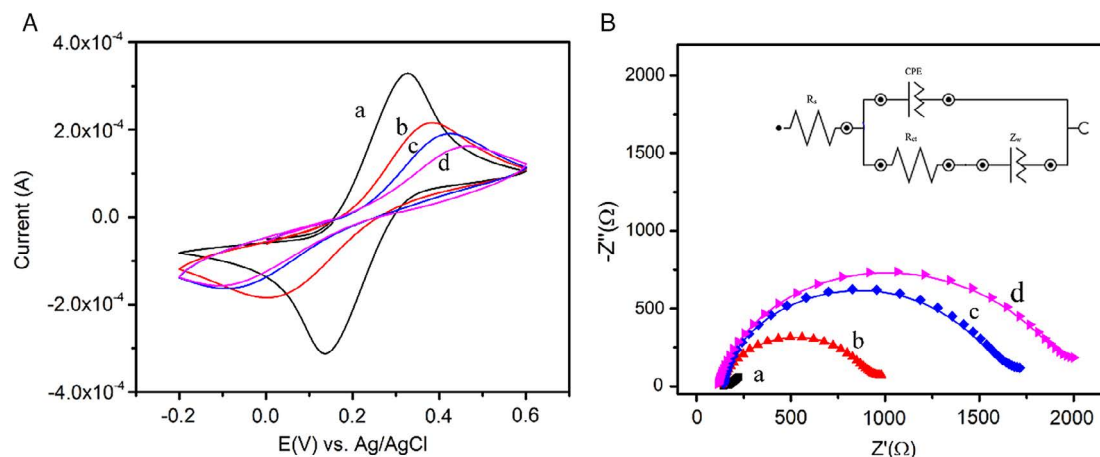
Figure 2. A) CV and B) EIS of differently modified electrodes in 0.1 M KCl solution containing 5×10^{-3} M $[Fe(CN)_6]^{3-/4-}$: a) the bare chip; b) S1/Au electrode; c) MCH/S1/Au electrode; d) MCH/S1/Au electrode in the presence of DA and S2. Inset in part (B) shows the equivalent circuit model with electrolyte resistance (R_s), the electron-transfer resistance (R_{et}), phase element (CPE), and a Warburg impedance.

the increase in the interfacial electron-transfer resistance (R_{et}) caused by the step-wise adsorption of receptor and backfill molecules. The impedance data were analyzed according to a Randles equivalent circuit containing the electrolyte resistance (R_s), the electron-transfer resistance (R_{et}), and the interface capacitance, used here as the constant phase element (CPE), which improved the fit of the impedance measurements due to the inhomogeneity of the electrode surface and a Warburg impedance accounting for the diffusion of the redox probes. As shown in Figure 2B, the bare gold chip presented a small semicircle diameter (curve a), indicating a very fast electron-transfer process. After immobilization of S1, R_{et} increased (curve b) due to the electrostatic repulsion between the negatively charged S1 and redox probe $[Fe(CN)_6]^{3-/4-}$. Subsequently, surface blocking with MCH led to a further increase in R_{et} (curve c). R_{et} also increased obviously (curve d) after the addition of DA and S2 due to steric hindrances of charge transfer caused by the presence of DA. These results were in accordance with the observed CV results and indicated that a mixed self-assembled monolayer of aptamer receptor and backfill molecules was formed and that DA is bound to such an electrode (**Table 1**).

2.2. Ratiometric Electrochemical Biosensor

To test the general feasibility of a ratiometric DA biosensor, square-wave voltammetry (SWV) responses of different modified gold chips were recorded. Firstly, the S1 strand was immobilized together with its complementary CS1 strands as well as MCH. Correspondingly, a high oxidation peak of AQ at about -0.6 V
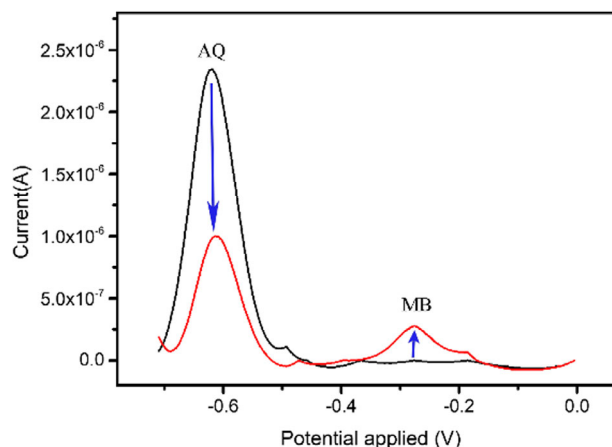
Table 1. EIS results of fitting experimental data to the equivalent circuit.

	R_s [Ω]	R_{et} [kΩ]
Bare chip	141	0.0216
S1/Au electrode	132	0.71
MCH/S1/Au electrode	142	1.20
MCH/S1/Au electrode in the presence of DA and S2	120	1.77

Figure 3. SWV response in the absence of DA (black curve) and in the presence of DA (30×10^{-6} M, 10×10^{-3} M PBS [pH 7.4, 2×10^{-3} M $MgCl_2$, 100×10^{-3} M NaCl]; red curve).

was exclusively observed in the absence of DA (curve black), indicating that S1 was successfully immobilized on the gold chip and hybridized with CS1 (**Figure 3**). Noteworthy, S2 was also present in the medium; however, no MB response was measured because DA was absent. However, after the addition of 30×10^{-6} M DA, the AQ signal obviously decreased, accompanied by the appearance of an additional MB redox signal (curve red). The drop of the AQ signal was caused by the formation of S1–DA–S2 complexes and the corresponding release of CS2 from the electrode surface. Furthermore, the MB signal indicates that the redox probe was close enough to the electrode surface to participate in the charge transfer. These results demonstrated the feasibility of a ratiometric electrochemical sensor scheme for the detection of DA.

2.3. Optimization of Detection Performance

To obtain the best performance for the ratiometric electrochemical biosensor, the ratiometric peak current (I_{MB}/I_{AQ}) in the
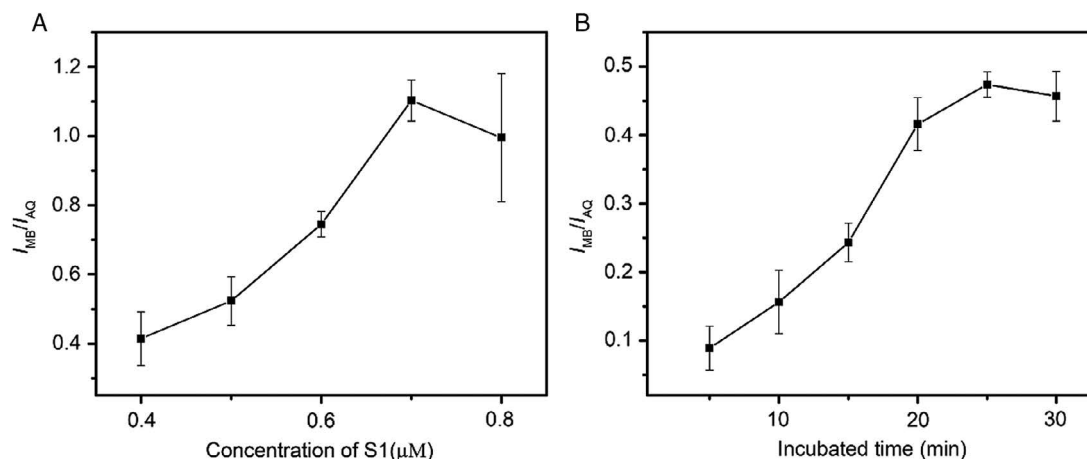
Figure 4. Effect of A) concentration of S1 and B) incubated time recorded for a concentration of DA of 50×10^{-6} M. Error bars represent standard deviations of three parallel experiments.

presence of 50×10^{-6} M DA was optimized with regard to the concentration of S1 and incubation time with target DA. As shown in **Figure 4**A, the ratio value increased with the increasing concentration of S1 from 0.4 to 0.7×10^{-6} M, followed by a slight decrease. Such a behavior is not unusual because high receptor densities at the surface can lead to steric hindrances between neighboring ssDNA stands and prevent further analyte binding. Therefore, a concentration of 0.7×10^{-6} M S1 was used in the following for the preparation of the ratiometric biosensor. Also, the incubation time of the analyte is typically an important parameter that has to be considered to ensure the optimal biosensor performance. From Figure 4B, one can see that the sensor signal continuously increased for the first 25 min and then leveled off, indicating that the DA binding saturated. Thus, 25 min was used as the incubation time for subsequent experiments. The concentration of DA was again 50×10^{-6} M.

2.4. Sensitivity of the Ratiometric Electrochemical Biosensor

To evaluate the sensitivity of the ratiometric electrochemical biosensor for the detection of DA, the SWV peak current ratio in response to different concentrations of DA was measured in the optimal experimental conditions mentioned previously. With increasing concentration of DA, the peak current of AQ decreased and that of MB increased correspondingly (**Figure 5**). Plotting the current signal versus the logarithm of the DA concentration for both I_{MB} and I_{AQ} resulted in an idealistic calibration curve for MB signal with a lower concentration limit defined by the LOD, a linear range of about one order of magnitude, and saturation at a concentration of 200×10^{-6} M. The narrow linear detection range of one order of magnitude and the moderate sensitivity ($0.38\,\mu A/\mathrm{dec}[C_{DA}]$) are presumably correlated to the overall small SWV currents that were measured for the binding of DA and the associated S2 strand. The small currents for MB in comparison with AQ (sensitivity of $1.5\,\mu A/\mathrm{dec}[C_{DA}]$) suggest that the distance between the MB redox probe and the electrode is relatively large for the formed S1–DA–S2 complex and therefore charge transfer is less efficient. On the contrary, the AQ redox probe is located in close proximity to the electrode surface according to the design of the CS1 strand (Figure 1). Correspondingly, the charge transfer is very efficient and the current signal was higher than that of MB, although both redox probes transfer the same number of charges ($2e^-$) during the detection process. To evaluate the final sensor performance, the two sensor signals can be logically interrelated in different ways. If a signal with high reliability is required, then the signals can be treated as logic gate inputs and linked by an AND logic gate. According to the truth table of this gate, the output will be different from zero only if both inputs are also nonzero. This means that only those values of the sensor are analyzed where both CS1-AQ and S2-MB signals are above the LOD. Consequently, uncertain situations caused by unspecific DA-free S2-MB signaling or signal drops of CS1-AQ due to electrode degradation can be eliminated from the data analysis. On the contrary, the ratio of I_{MB}/I_{AQ} can be calculated as well. Here, the increasing *on signal* generated by S2 is divided by the decreasing *off signal* that originating from the demerged CS1 strands. This scenario corresponds to a logic OR gate, where the out signal is different from zero if either CS1, S2, or both are nonzero. Consequently, any change in the redox signal is used for data analysis. This can extend the dynamic range of detection and increase the sensor sensitivity however it reduces the reliability. In the current case, the value of the redox signal ratio showed a linear relationship for the log of the DA concentration in a range from 20 to 350×10^{-6} M (larger than CS1 and S2 responses) with a sensitivity of $3.5\,\mu A/\mathrm{dec}[C_{DA}]$. The LOD (actual measurement) was 10×10^{-6} M.

2.5. Selectivity and Regeneration of Ratiometric Electrochemical Aptasensor

To investigate the selectivity of the ratiometric electrochemical biosensor, we chose ascorbic acid (AA) and uric acid (UA) as competing substances because they are interfering electroactive compounds that coexist with DA in relevant biological samples. The SWV peak current ratio was monitored in response to DA, AA, UA, and a mixture of them, respectively. As shown
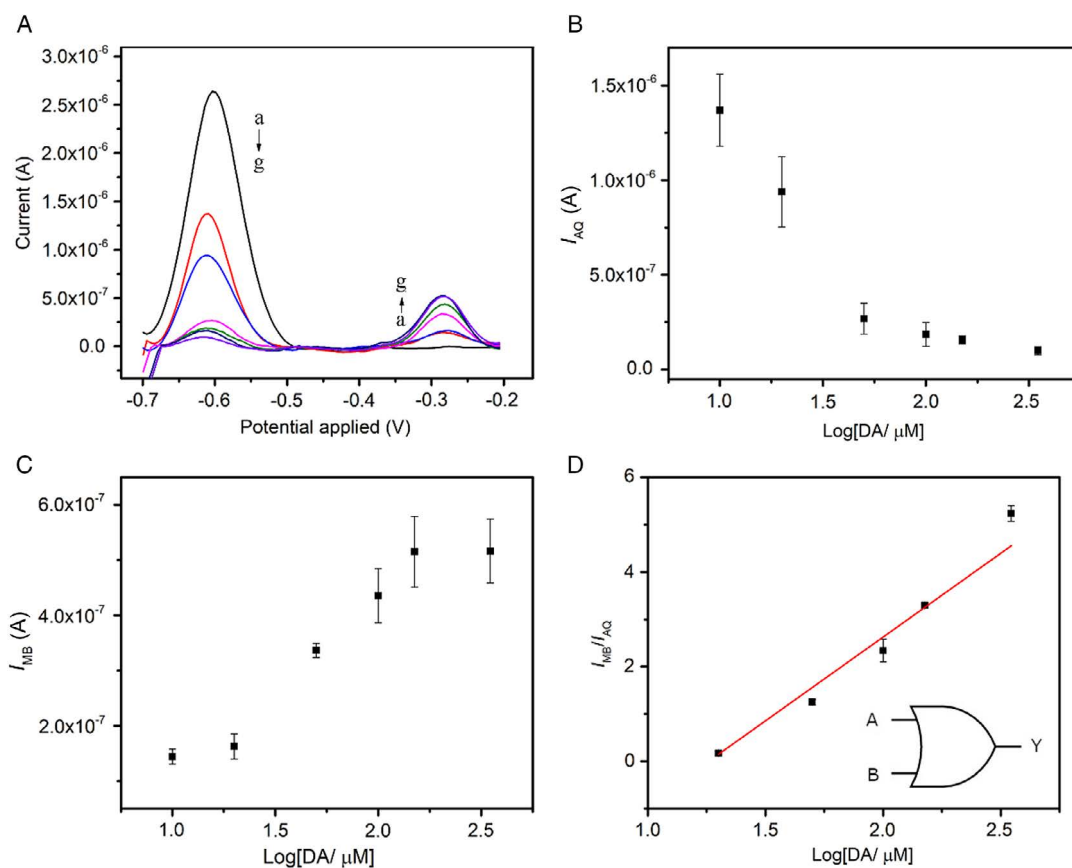
Figure 5. A) SWV curves recorded for different concentrations of DA: a) 0×10^{-6} M, b) 10×10^{-6} M, c) 20×10^{-6} M, d) 50×10^{-6} M, e) 100×10^{-6} M, f) 200×10^{-6} M, and g) 350×10^{-6} M. B) The logarithmic dependence of the AQ signal on the concentration of DA. C) The logarithmic dependence of the MB signal on the concentration of DA. D) The logarithmic dependence of the SWV current peak ratio of I_{MB}/I_{AQ} on the concentration of DA. Error bars represent the standard deviations of three parallel experiments. Inset: symbol of an OR logic gate where A and B represent the redox signals of CS1 and S2, respectively, whereas Y is the ratio of both I_{MB}/I_{AQ}.
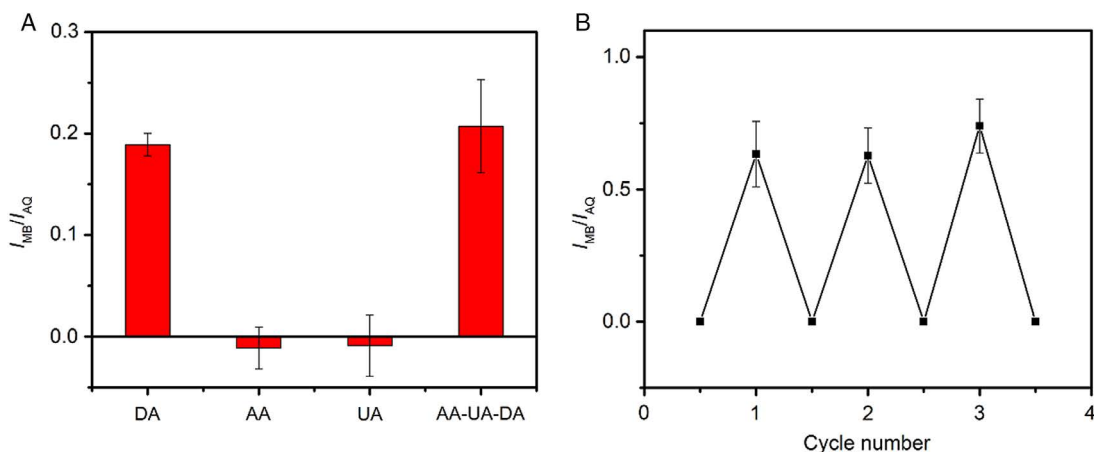

Figure 6. A) Selectivity of the ratiometric biosensor for DA. DA (20×10^{-6} M), AA (200×10^{-6} M), and UA (200×10^{-6} M) were chosen. B) Regeneration of the ratiometric electrochemical biosensor. Error bars represent standard deviations of three parallel experiments.

in **Figure 6**, a high signal ratio was obtained in the presence of 20×10^{-6} M DA in comparison with the interfering compounds, which were tested at the same concentration. Even if

AA and UA are mixed with DA in ten times excess (200×10^{-6} M AA and UA vs 20×10^{-6} M DA), the sensor signal corresponds to the response obtained for DA alone. This result

Table 2. Recovery and relative standard deviation (RSD) of DA in diluted human serum with the developed ratiometric biosensor.

Add [$\times 10^{-6}$ M]	Recovery [%]	RSD [%]
20	105	6.5
50	88	18

indicates that our split aptasensor exhibits an excellent selectivity for the detection of DA and that AA and UA do not interfere with DA binding. Furthermore, Nakatsuka et al. reported that the full aptamer which was split in this work showed negligible responses to norepinephrine, serotonin, L-3,4-dihydroxyphenylalanine (L-DOPA), homovanillic acid, 3-methoxytyramine, tyramine, and 3,4-dihydroxyphenylacetic acid (DOPAC).[40] The reason for this superior selectivity is based on the SELEX process, where serotonin, tyrosine, and L-DOPA were used as countertargets.

Although device accuracy, selectivity, sensitivity, and response time are the major characteristics of DA sensors, the reusability of aptasensors can also become an advantage over immunosensors due to sustainability and waste prevention.[41,42] Therefore, we tested the regeneration capability of our electrochemical biosensor. The ratiometric biosensor was reactivated after each successful analyte detection experiment by incubating the sensor in a high concentration salt solution of 2 M NaCl for 5 min to dissociate the S1–DA–S2 complex and release the analyte molecule. Afterward, the detection experiment was performed again with the same DA concentration of 30×10^{-6} M. Rerunning this regeneration process three times resulted in a reproducible detection response for DA, demonstrating the regeneration capability of this biosensor. It is noteworthy that the current ratio I_{MB}/I_{AQ} dropped to almost zero after regeneration with 2 M NaCl solution, demonstrating that the mixed monolayer suppresses the unspecific adsorption of S2. The recovery of the ratio after the addition of DA indicates furthermore that electrofouling of DA on the electrode surface was prevented, which is a common problem for all types of DA sensors. The aptasensor benefits in this regard from the cathodic redox potentials of MB and AQ, which are both distinctly more negative than the redox potential of DA. Consequently, electro-oxidation of DA and polydopamine formation was avoided, which possesses a robust adhesion capability to virtually all types of surfaces.[43]

To evaluate the application of the ratometric electrochemical biosensor in a sample with a more complex matrix (relative to cell culture medium), DA was added to the human serum samples, and recovery experiments for DA were conducted. Therefore, the human serum samples were diluted 1:500 by mixing it with 10×10^{-3} M PBS (pH 7.4, 2×10^{-3} M MgCl$_2$, 100×10^{-3} M NaCl). The detection results are shown in **Table 2**. The recoveries were in the range from 88% to 105%. These results demonstrate a high accuracy of our electrochemical biosensor for DA in diluted human serum samples.

3. Conclusion

In summary, a novel ratiometric electrochemical biosensor for the detection of DA has been successfully developed, which

potentially can be used for the in vitro measurement of neurotransmitter release from dopaminergic cells or for drug testing. Therefore, we split the aptamer into two fragments. One part (S1) was modified with a thiol linker and immobilized on the gold sensor surface. In addition, a short DNA strand CS1 complementary to S1 was designed, which was tagged with a redox probe AQ reporting on the amount of the target-free aptamer strand S1 attached on the surface. The second strand S2 of the aptamer was modified with a MB redox probe and has the capability to form S1–DA–S2 complexes on the sensor surface, reporting on the concentration of DA in the solution. Combining both redox signals by applying AND or OR logic gate operations resulted in an improvement of sensor reliability or enlarged detection range in comparison with a single signal alone. Furthermore, this ratiometric electrochemical biosensor possessed excellent selectivity and can be regenerated for multiple uses without losing sensitivity. Our work demonstrates that the electrochemical ratiometric detection can be easily implemented for split atpamer sensors and contribute to an improvement of sensor reliability and sensitivity.

4. Experimental Section

Chemicals: MCH, hydrochlorides DA, AA, UA, tris phosphine hydrochloride (TECP), 6-potassium ferricyanide [K$_3$Fe(CN)$_6$], potassium ferrocyanide [K$_4$Fe(CN)$_6$·4H$_2$O], and human serum were obtained from Sigma-Aldrich. All aqueous solutions were prepared using Milli-Q water (18.2 MΩ, Milli-Q, Millipore). The ssDNA molecules were purchased from FRIZ Biochem GmbH. S1: TTC GCA GGT GTG GAG TGA CGT CG-(CH$_2$)$_6$-SH; CS1: AQ-(CH$_2$)$_6$-CG ACG TAA CTG GAC ACC; S2: MB-(CH$_2$)$_6$-CGA CGC CAG TTT GAA GGT TCG. Each ssDNA sequence was modified with an alkyl chain between the oligonucleotide and thiol group/redox probe to prevent undesired phase separation between aptamer and MCH backfill as well as reduce interfering interactions between redox tag and nucleotides.

Instrumental Setup: Gold chips were prepared in the Helmholtz Nanoelectronic facility (HNF) of Forschungszentrum Jülich, by growing a 400 nm thermal silicon oxide dielectric interlayer on 4 in. silicon wafers, which were purchased from Si-Mat. Subsequently, a metal stack of the 10 nm titanium adhesion layer and 100 nm gold layer was deposited using electron beam evaporation (Pfeiffer Vacuum PLS570, Germany). The waver was diced into 1 cm × 1 cm pieces and the resulting gold chips were cleaned in a plasma oven (Diener Electronic, Germany). All electrochemical measurements were carried out on an Autolab potentiostat/galvanostat PGSTAT302 (Eco Chemie, the Netherlands) equipped with NOVA 2.01 software. A conventional three-electrode cell was used with a gold chip as the working electrode, Ag/AgCl electrode as the reference electrode, and Pt wire as the counterelectrode. DNA sequence concentrations were determined at 260 nm with the UV/vis/NIR spectrometer Lambda 900 (Perkin Elmer, USA).

Fabrication of Electrochemical Biosensor: Prior to modification, the gold chip should be clean. First, the gold chip was sonicated with acetone and isopropanol for 5 min, followed by rinsing with Milli-Q water and drying in a N$_2$ stream. Then, the gold chip underwent oxygen plasma treatment (O$_2$ pressure 0.5 mbar, 50% power, 5 min). Finally, the gold chips were immersed in ethanol for 30 min to reduce the formed gold oxides and dried with N$_2$.

Before immobilization of the receptor molecules on the gold transducer surface, 0.5×10^{-6} M of the thiol-tagged aptamer strand S1 was pretreated with 10×10^{-3} M TCEP for 1 h to cleave the disulfide bonds. The gold chip was incubated with S1 at room temperature for 16 h to immobilize the molecules on the gold chip through Au-S bonds. The gold chip was then thoroughly rinsed with 10×10^{-3} M PBS (pH 7.4, 100×10^{-3} M NaCl) buffer for the removal of nonbonded S1. Subsequently, the gold chip was incubated with 1×10^{-3} M MCH ethanol solution for 1 h to block

the unmodified sites and suppress unspecific binding. Finally, the modified gold chip was rinsed thoroughly with PBS buffer. To monitor each immobilization step, the corresponding CV and EIS were conducted in 0.1 M KCl solution with 5×10^{-3} M ferri-/ferro-cyanide as the redox probe.

Detection of DA: The S1-modified chip was immersed in 10×10^{-3} M PBS (pH 7.4, 2×10^{-3} M MgCl$_2$, 100×10^{-3} M NaCl), containing S2 and CS1. Different concentrations of DA were added. The electrochemical SWV responses were measured by scanning the potential from -0.5 to 0 V with a pulse frequency of 5 Hz.

Acknowledgements

Conflict of Interest

The authors declare no conflict of interest.

Keywords

[1] A. L. Sun, Y. F. Zhang, G. P. Sun, X. N. Wang, D. Tang, *Biosens. Bioelectron.* **2017**, *89*, 659.

[2] Y. Wu, R. Lai, *Anal. Chem.* **2016**, *88*, 2227.

[3] S. Wang, L. Q. Zhang, S. Wan, S. Cansiz, C. Cui, Y. Liu, R. Cai, C. Hong, I. T. Teng, M. Shi, Y. Wu, *ACS Nano* **2017**, *11*, 3943.

[4] M. H. Lin, P. Song, G. Zhou, X. Zuo, A. Aldalbahi, X. Lou, J. Shi, C. Fan, *Nat. Protoc.* **2016**, *11*, 1244.

[5] B. T. Dou, B. Xu, B. Jiang, R. Yuan, Y. Xiang, *Anal. Chem.* **2019**, *91*, 10792.

[6] Y. Zheng, X. Y. Wang, S. He, Z. Gao, Y. Di, K. Lu, K. Li, J. Wang, *Biosens. Bioelectron.* **2019**, *126*, 261.

[7] S. H. Yu, C. S. Lee, T. H. Lim, *Nanomaterials* **2019**, *9*, 817.

[8] S. M. Taghdisi, N. M. Danesh, M. A. Nameghi, M. Ramezani, M. Alibolandi, K. Abnous, *Biosens. Bioelectron.* **2019**, *133*, 230.

[9] D. P. Sun, J. Lu, L. Zhang, Z. Chen, *Anal. Chim. Acta* **2019**, *1082*, 1.

[10] E. Paleček, K. M. Bartoší, *Chem. Rev.* **2012**, *112*, 3427.

[11] C. H. Fan, K. W. Plaxco, A. J. Heeger, *Proc. Natl. Acad. Sci.* **2003**, *100*, 9134.

[12] Y. Xiao, A. A. Lubin, A. J. Heeger, K. W. Plaxco, *Angew. Chem. Int. Ed.* **2005**, *44*, 5456.

[13] X. L. Zuo, S. P. Song, J. Zhang, D. Pan, L. Wang, C. Fan, *J. Am. Chem. Soc.* **2007**, *129*, 1042.

[14] B. R. Baker, R. Y. Lai, M. S. Wood, E. H. Doctor, A. J. Heeger, K. W. Plaxco, *J. Am. Chem. Soc.* **2006**, *128*, 3138.

[15] Z. G. Yu, R. Y. Lai, *Talanta* **2018**, *176*, 619.

[16] Z. G. Yu, A. L. Sutlief, R. Y. Lai, *Sens. Actuators B* **2018**, *258*, 722.

[17] X. L. Zuo, Y. Xiao, K. W. Plaxco, *J. Am. Chem. Soc.* **2009**, *131*, 6944.

[18] Z. G. Yu, R. Y. Lai, *Chem. Commun.* **2012**, *48*, 10523.

[19] L. Cui, M. F. Lu, Y. Li, B. Tang, C. Y. Zhang, *Biosens. Bioelectron.* **2018**, *102*, 87.

[20] Y. J. Cui, R. J. Song, J. Yu, M. Liu, Z. Wang, C. Wu, Y. Yang, Z. Wang, B. Chen, G. Qian, *Adv. Mater.* **2015**, *27*, 1420.

[21] M. H. Lee, J. S. Kim, J. Sessler, *Chem. Soc. Rev.* **2015**, *44*, 4185.

[22] J. K. Deng, Y. Q. Liu, X. Lin, Y. Lyu, P. Qian, S. Wang, *Sens. Actuators B* **2018**, *273*, 1495.

[23] Q. Xiao, J. R. Feng, M. Feng, J. Li, Y. Liu, D. Wang, S. Huang, *Microchim. Acta* **2019**, *186*, 478.

[24] H. Jin, C. Q. Zhao, R. Gui, X. Gao, Z. Wang, *Anal. Chim. Acta* **2018**, *1025*, 154.

[25] W. J. Shen, Y. Zhuo, Y. Q. Chai, R. Yuan, *Anal. Chem.* **2015**, *87*, 11345.

[26] C. X. Zhu, M. Y. Liu, X. Li, X. Zhang, J. Chen, *Chem. Commun.* **2018**, *54*, 10359.

[27] Y. N. Zhang, S. Guo, S. Cheng, X. Ji, Z. He, *Biosens. Bioelectron.* **2017**, *94*, 478.

[28] H. Li, N. Arroyo-Curras, D. Kang, F. Ricci, K. W. Plaxco, *J. Am. Chem. Soc.* **2016**, *138*, 15809.

[29] X. Li, B. T. Dou, R. Yuan, Y. Xiang, *Sens. Actuators B* **2019**, *286*, 191.

[30] H. K. Walter, J. Bauer, J. Steinmeyer, A. Kuzuya, C. M. Niemeyer, H. A. Wagenknecht, *Nano Lett.* **2017**, *17*, 2467.

[31] L. Y. Shen, T. Bing, X. J. Liu, J. Wang, L. Wang, N. Zhang, D. Shangguan, *Interfaces* **2018**, *10*, 2312.

[32] H. X. Yu, J. Canoura, B. Guntupalli, X. Lou, Y. Xiao, *Chem. Sci.* **2017**, *8*, 131.

[33] X. F. Zheng, R. Z. Peng, X. Jiang, Y. Wang, S. Xu, G. Ke, T. Fu, Q. Liu, S. Huan, X. Zhang, *Anal. Chem.* **2017**, *89*, 10941.

[34] L. Feng, A. Sivanesan, Z. Lyu, A. Offenhäusser, D. Mayer, *Biosens. Bioelectron.* **2015**, *66*, 62.

[35] L. Feng, Z. Lyu, A. Offenhäusser, D. Mayer, *Angew. Chem. Int. Ed.* **2015**, *54*, 7693.

[36] D. S. Goldstein, C. Holmes, Y. Sharabi, *Brain* **2012**, *135*, 1900.

[37] R. M. Wightman, L. J. May, A. C. Michael, *Anal. Chem.* **1988**, *60*, 769A.

[38] K. Jackowska, P. Krysinski, *Anal. Bioanal. Chem.* **2013**, *405*, 3753.

[39] D. S. Kim, E. S. Kang, S. Baek, S. S. Choo, Y. H. Chung, D. Lee, J. Min, T. H. Kim, *Sci. Rep.* **2018**, *8*, 14049.

[40] N. Nakatsuka, K. A. Yang, J. M. Abendroth, K. M. Cheung, X. Xu, H. Yang, C. Zhao, B. Zhu, Y. S. Rim, Y. Yang, P. S. Weiss, *Science* **2018**, *362*, 319.

[41] G. Figueroa-Miranda, L. Feng, S. C. Shiu, R. M. Dirkzwager, Y. W. Cheung, J. A. Tanner, M. J. Schöning, A. Offenhäusser, D. Mayer, *Sens. Actuators B* **2018**, *255*, 235.

[42] Y. Zhang, G. Figueroa-Miranda, Z. Lyu, C. Zafiu, D. Willbold, A. Offenhäusser, D. Mayer, *Sens. Actuators B* **2019**, *288*, 535.

[43] E. Petola, S. Sainio, K. B. Holt, T. Palomäki, J. Koskinen, T. Laurila, *Anal. Chem.* **2018**, *90*, 1408.